

Dicer1 Deficiency in the Idiopathic Pulmonary Fibrosis Fibroblastic Focus Promotes Fibrosis by Suppressing MicroRNA Biogenesis

Jeremy Herrera¹, Daniel J. Beisang², Mark Peterson¹, Colleen Forster³, Adam Gilbertsen¹, Alexey Benyumov¹, Karen Smith¹, Christopher E. Korenczuk⁴, Victor H. Barocas⁴, Kacey Guenther¹, Ryan Hite¹, Lin Zhang⁵, Craig A. Henke¹, and Peter B. Bitterman¹

¹Department of Medicine, ²Department of Pediatrics, ³Clinical and Translational Science Institute, Biorepository & Laboratory Services, Histology and Research Laboratory, ⁴Department of Biomedical Engineering, and ⁵Division of Biostatistics, School of Public Health, University of Minnesota, Minneapolis, Minnesota

ORCID ID: 0000-0002-7995-7117 (P.B.B.).

Abstract

Rationale: The lung extracellular matrix (ECM) in idiopathic pulmonary fibrosis (IPF) mediates progression of fibrosis by decreasing fibroblast expression of miR-29 (microRNA-29), a master negative regulator of ECM production. The molecular mechanism is undefined. IPF-ECM is stiffer than normal. Stiffness drives fibroblast ECM production in a YAP (yes-associated protein)-dependent manner, and YAP is a known regulator of miR-29. Therefore, we tested the hypothesis that negative regulation of miR-29 by IPF-ECM was mediated by mechanotransduction of stiffness.

Objectives: To determine how IPF-ECM negatively regulates miR-29.

Methods: We decellularized lung ECM using detergents and prepared polyacrylamide hydrogels of defined stiffness by varying acrylamide concentrations. Mechanistic studies were guided by immunohistochemistry of IPF lung and used cell culture, RNA-binding protein assays, and xenograft models.

Measurements and Main Results: Contrary to our hypothesis, we excluded fibroblast mechanotransduction of ECM stiffness as the primary mechanism deregulating miR-29. Instead, systematic examination of miR-29 biogenesis revealed a microRNA processing defect that impeded processing of miR-29 into its mature bioactive forms. Immunohistochemical analysis of the microRNA processing machinery in IPF lung specimens revealed decreased Dicer1 expression in the procollagen-rich myofibroblastic core of fibroblastic foci compared with the focus perimeter and adjacent alveolar walls. Mechanistically, IPF-ECM increased association of the Dicer1 transcript with RNA binding protein AUF1 (AU-binding factor 1), and Dicer1 knockdown conferred primary human lung fibroblasts with cell-autonomous fibrogenicity in zebrafish and mouse lung xenograft models.

Conclusions: Our data identify suppression of fibroblast Dicer1 expression in the myofibroblast-rich IPF fibroblastic focus core as a central step in the mechanism by which the ECM sustains fibrosis progression in IPF.

Keywords: idiopathic pulmonary fibrosis; extracellular matrix; yes-associated protein

(Received in original form September 6, 2017; accepted in final form March 26, 2018)

Supported by the NIH grants R01 HL125236 (P.B.B.), P01 HL091775 and R01 HL125227 (C.A.H.), and T32 HL077410 (J.H. and D.J.B.); National Center for Advancing Translational Sciences grant UL1TR000114 (C.F.); National Science Foundation Graduate Research Fellowship Program grant 00039202 (C.E.K.); and funds provided by the O'Brien and Witowski families. C.E.K. is a recipient of the Richard Pyle Scholar Award from the Achievement Rewards for College Scientists Foundation.

Author Contributions: J.H. and K.G. conducted the experiments with decellularized extracellular matrix. D.J.B. designed and conducted the RNA binding protein measurements. J.H., K.G., and R.H. conducted the experiments with hydrogels. J.H. and A.G. performed the mouse experiments. J.H. and A.B. conducted the zebrafish experiments. K.S. developed and validated all lentiviral constructs. J.H., C.E.K., and V.H.B. performed the uniaxial tensile strain measurements. J.H. and M.P. prepared and validated primary fibroblast cell lines and extracellular matrix preparations. J.H. and C.F. performed all the histological stains. L.Z. performed statistical analysis for the study. J.H. and P.B.B. wrote the manuscript with input from all authors. J.H., C.A.H., and P.B.B. conceived the project, and P.B.B. supervised all experiments.

Correspondence and requests for reprints should be addressed to Peter B. Bitterman, M.D., Division of Pulmonary, Allergy, Critical Care and Sleep Medicine, University of Minnesota, 420 Delaware Street SE, MMC 276, Minneapolis, MN 55455. E-mail: bitte001@umn.edu.

This article has an online supplement, which is accessible from this issue's table of contents at www.atsjournals.org.

Am J Respir Crit Care Med Vol 198, Iss 4, pp 486–496, Aug 15, 2018

Copyright © 2018 by the American Thoracic Society

Originally Published in Press as DOI: 10.1164/rccm.201709-1823OC on March 26, 2018

Internet address: www.atsjournals.org

At a Glance Commentary

Scientific Knowledge on the

Subject: The lung extracellular matrix in idiopathic pulmonary fibrosis is fibrogenic, but the molecular mechanisms have not been elucidated.

What This Study Adds to the

Field: Here we show that the lung extracellular matrix in idiopathic pulmonary fibrosis mediates fibrosis progression by suppressing myofibroblast expression of Dicer1 in the core region of the fibroblastic focus, thus decreasing the biogenesis of miR-29, a master negative regulator of stromal genes.

Idiopathic pulmonary fibrosis (IPF) is a relentlessly progressive form of lung scarring. Available data indicate that IPF lung extracellular matrix (ECM) itself is fibrogenic (1–3). Fibroblasts cultured on decellularized IPF lung ECM (IPF-ECM) suppresses expression of miR-29 (microRNA-29) (a master negative regulator of stromal genes), leading to increased ribosome recruitment to hundreds of stromal genes, including: collagens, fibronectin, and their cognate integrins; matrix metalloproteinases; and proteins controlling proliferation and motility. Restoration of fibroblast miR-29 expression returns translation of miR-29 target genes back to baseline (3). Although miR-29 suppression has been established in IPF (4) and other fibrotic disorders (5–8) for several years; the underlying mechanisms remain unknown. Here we set out to unveil the molecular mechanism by which IPF-ECM decreases fibroblast miR-29 expression.

Identifying the ECM properties sensed by fibroblasts to suppress miR-29 has the potential to unveil new targets that can be exploited to develop therapies that interrupt fibrosis progression. One signature property of IPF lung ECM that distinguishes it from normal is its elastic modulus (stiffness). IPF lung ECM is up to an order of magnitude stiffer than normal, with steep stiffness gradients between fibrotic and morphologically uninvolved regions of the lung (1, 9). Mechanotransduction of ECM stiffness has prominent roles in pathological processes, including cancer

progression and fibrosis (9–12). Expression of the mechanosensitive Hippo pathway constituent YAP (yes-associated protein) is increased in the IPF lung, and ectopic expression of activated YAP confers fibroblasts with fibrogenic properties, including increased ECM production (9). YAP has dual functions with diametric effects on miR-29 expression. At the single-gene level, YAP serves as a transcriptional coactivator of *miR-29b-1/a* (13), the gene encoding miR-29a and miR-29b-1; two of the three molecular species of miR-29 (a separate gene on chromosome 1 encodes miR-29b-2 [identical to miR-29b-1, together designated miR-29b] and miR-29c). In contrast, on a genome-wide level, YAP functions as a negative regulator of microRNA expression by sequestering p72, an integral component of the microRNA processing machinery (14). Thus, mechanotransduction of ECM stiffness leading to activation of YAP

provides a plausible molecular mechanism by which IPF-ECM regulates miR-29.

To explore this possibility, we combined *in situ* analysis of IPF lung tissue with experiments using primary human lung fibroblasts studied on decellularized human lung ECM, ECM functionalized hydrogels of tunable stiffness, and two xenograft models. Although stiff hydrogels triggered fibroblast YAP activation and increased miR-29 expression, decellularized IPF-ECM did exactly the opposite, excluding mechanotransduction of stiffness through YAP as the primary mechanism. Instead, we discovered that IPF-ECM suppresses microRNA biogenesis at the processing step by downregulating Dicer1 (an integral microRNA processing component) in the myofibroblast core of the fibroblastic focus, where active ECM synthesis is taking place. Dicer1 deficiency in primary lung fibroblasts decreased mature miR-29 levels and increased

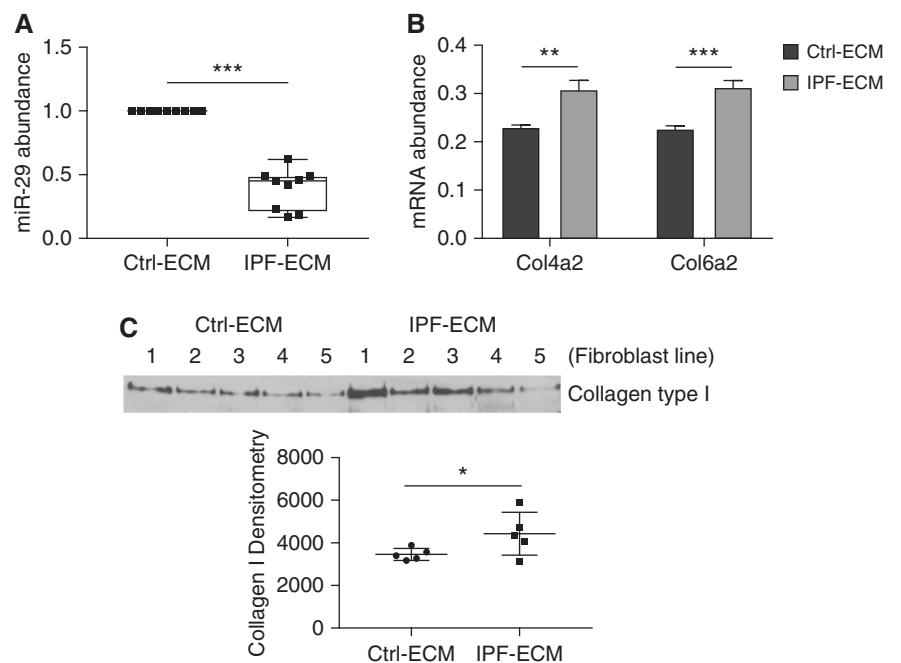


Figure 1. Idiopathic pulmonary fibrosis (IPF)–extracellular matrix (ECM) suppresses miR-29 (microRNA-29) expression and upregulates collagen production. Lung fibroblasts were cultured on control or IPF-ECM for 18 hours. (A) Mature miR-29a, -29b, and -29c values were quantified by quantitative PCR (qPCR) and normalized to RNU6 ($n = 1$ cell line). Shown is a box-and-whisker plot representing the mean of three technical replicates for the three species of miR-29 with the values for control (Ctrl)-ECM set to 1. (B) qPCR for Col4a2 and Col6a2 normalized to GAPDH ($n = 2$, representative experiment shown), and P value was calculated using the Student's two-tailed t test. (C) Medium was removed and equal volumes of serum-free medium were added to each reaction. After 8 hours, the conditioned medium was collected and equal volumes analyzed by immunoblot for type I collagen ($n = 5$ cell lines, densitometry values shown in graph below). Error bars represent mean \pm SD. P value was calculated using the Student's two-tailed t test for A and B, and paired two-tailed t test for C. * $P < 0.05$, ** $P < 0.01$, *** $P < 0.005$.

collagen expression on control-ECM (enforced Dicer1 expression was toxic, precluding gain-of-function studies on IPF-ECM). We established a definitive mechanistic link to Dicer1 deficiency by showing that in both zebrafish and mouse xenografts, Dicer1 deficiency conferred human lung fibroblasts with cell-autonomous fibrogenicity. Our data show for the first time that ECM-mediated suppression of fibroblast Dicer1 in the myofibroblast core of the fibroblastic focus is a central step in IPF disease progression by decreasing the processing of precursor miR-29 into its mature antifibrotic forms. This finding provides foundational new knowledge that paves the way for developing novel precision therapeutics targeting fibrosis progression. Some of the results presented here have been previously reported in abstract form (15).

Methods

Detailed methods can be found in the online supplement.

Statistical Analysis

For analyses of data with sample sizes greater than six, one-sample or two-sample *t* tests were used for hypothesis testing on the means of the distributions. For analyses of data with sample sizes less than six, nonparametric tests such as the Wilcoxon rank sum test were used to test the medians of distributions. For miR-29 abundance data under conditions of YAP overexpression, a Kruskal-Wallis test was used for a nonparametric one-way ANOVA test followed by a Tukey test for pairwise comparisons with the *P* values adjusted for the multiple comparisons. For analysis of AUF-1 pull-down data, a one-sided Mann-Whitney *U* test was used. All analyses and plots were conducted in Prism.

Results

IPF-ECM Suppresses miR-29 Expression and Upregulates Collagen Production

Prior work using atomic force microscopy indicates that regions of the IPF-ECM are up to an order of magnitude stiffer than control-ECM (Ctrl-ECM) (1). To interrogate the ECM at a scale approximating the size of the human lung acinus (3 mm × 10 mm × 5 mm), we quantified uniaxial tensile strain in lung tissue strips and found

IPF-ECM to be significantly stiffer than Ctrl-ECM at this scale of resolution (see Figure E1 in the online supplement). Our prior studies indicate that IPF-ECM suppresses miR-29 family member expression in human lung fibroblasts (3). We reexamined this effect with methodological refinements designed to minimize the effect of serum growth factors (low-serum survival medium) and controlled for patient-to-patient and lung ECM heterogeneity (Ctrl-ECM preparations from three patients or IPF-ECM preparations from three patients in each reaction). Under these more stringent conditions, IPF-ECM significantly decreased all miR-29 species (Figure 1A). We next sought to determine whether relevant outside-in signaling pathways mediated this response. Pharmacologic agents inhibiting Notch (DAPT), PI3 kinase (LY294002), Rock/Rho (Y27632), Erk (SCH727294), focal adhesion kinase (PF562271), ALK5 (A83-01), or MTRF (CCG-100602) did not consistently restore fibroblast miR-29 levels on IPF-

ECM (Figure E2). As a positive control, we examined previously verified miR-29 stromal targets (type IV collagen and type VI collagen mRNA [3]; and type I collagen protein secretion) in fibroblasts on IPF-ECM. As expected, suppression of miR-29 by IPF-ECM increased expression of these miR-29 target genes (Figures 1B and 1C; Figure E3).

Stiffness Increases miR-29 Expression on Two-Dimensional Hydrogels

To determine whether stiffness and/or composition could account for the suppression of miR-29 expression on IPF-ECM, we cultured lung fibroblasts on synthetic two-dimensional (2D) polyacrylamide hydrogels (PA gels) of physiological stiffness (soft PA gels ~3 kPa) or IPF stiffness (stiff PA gels ~20 kPa). To validate our model system, we analyzed the impact of stiffness on α -smooth muscle actin expression. In accord with published data (9, 16), lung fibroblasts displayed increased α -smooth muscle actin on stiff

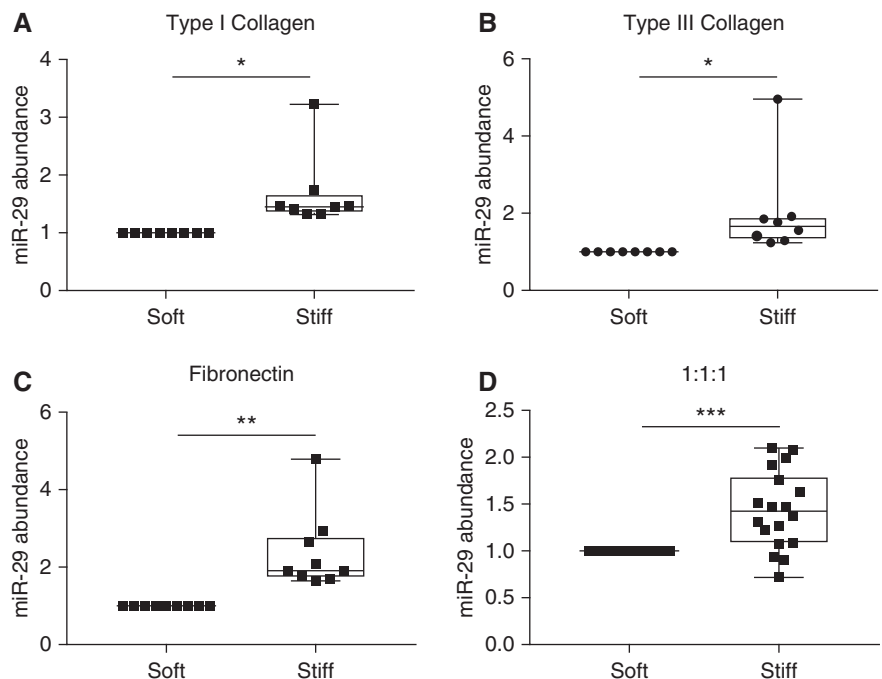


Figure 2. Stiffness increases miR-29 (microRNA-29) expression in two-dimensional hydrogels. Primary lung fibroblasts were cultured for 24 hours in survival medium on gels mimicking physiological stiffness (3 kPa; soft polyacrylamide gels) or gels mimicking idiopathic pulmonary fibrosis stiffness (20 kPa; stiff polyacrylamide gels). Gels were functionalized with either: (A) type I collagen (*n* = 3 cell lines); (B) type III collagen (*n* = 3 cell lines); (C) fibronectin (*n* = 3 cell lines); or (D) an equal ratio of type I collagen, type III collagen, and fibronectin (*n* = 6 cell lines). Shown is a box-and-whisker plot of the mean quantitative PCR values on stiff hydrogels compared with soft (set to 1) for miR-29a, -29b, and -29c (normalized to RNU6 expression). *P* values were calculated using the Student's paired two-tailed *t* test. **P* < 0.05, ***P* < 0.01, ****P* < 0.001.

PA gels functionalized with type I collagen (Figure E4). We next examined the effect of stiffness on miR-29 expression and were surprised to find that fibroblast miR-29 expression was increased by stiff PA gels functionalized with type I collagen, pointing away from stiffness *per se* as the property of IPF-ECM downregulating miR-29 (Figure 2A). The PA gel system is versatile, as it allows the gels to be functionalized by coating with any ECM

protein (17). To test the relative importance of stiffness versus composition in regulating miR-29, we supplemented the collagen I data by coating PA gels with collagen III alone, fibronectin alone, or an equal ratio of collagen I, collagen III, and fibronectin. Independent of substratum composition, stiffness consistently upregulated mature miR-29 abundance (Figures 2B–2D), revealing the primacy of stiffness over composition in the 2D hydrogel model.

IPF-ECM Negatively Regulates YAP and Suppresses miR-29 Transcription

We next sought to determine whether there was a causal role for YAP in the regulation of miR-29 by IPF-ECM. In accord with prior work (9), when fibroblasts resided on stiff 2D hydrogels, YAP nuclear localization (active YAP) and two canonical YAP transcriptional targets, which serve as readouts of YAP function, all increased (Figure E5). Contrary to expectation, when

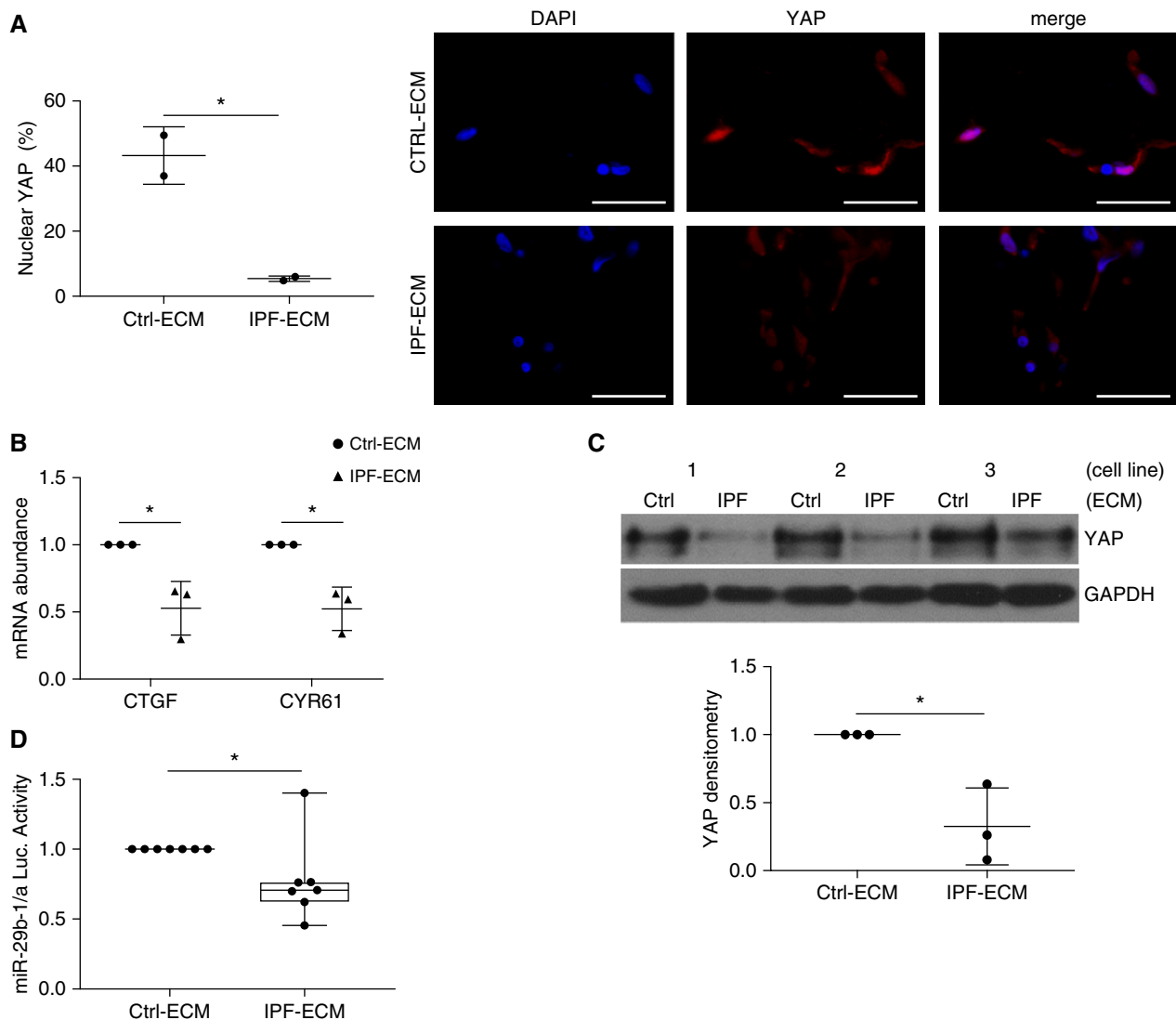


Figure 3. Idiopathic pulmonary fibrosis (IPF)–extracellular matrix (ECM) negatively regulates YAP (yes-associated protein) and suppresses miR-29 (microRNA-29) transcription. (A–C) Fibroblasts were cultured for 24 hours on ECM and (A) (left panel) nuclear YAP (percentage positive cells) was quantified by immunofluorescence microscopy ($n = 2$ cell lines, mean values shown); (right panel) representative image shown with scale bars representing $50 \mu\text{m}$. (B) Quantitative PCR for CTGF and CYR61 (normalized to GAPDH; $n = 3$ cell lines, mean values shown normalized to control [Ctrl]–ECM [set to 1]). (C) YAP expression was quantified by immunoblot (normalized to GAPDH; using three cell lines designated 1, 2, and 3; mean values shown normalized to Ctrl-ECM [set to 1]). Mean densitometry values are shown in lower panel. (D) Fibroblasts transfected with an miR-29b-1/a firefly luciferase reporter were cultured for 24 hours on ECM, and luciferase activity was quantified (normalized to Renilla luciferase; $n = 7$ cell lines shown as a box-and-whisker plot, mean value shown normalized to Ctrl-ECM [set to 1]). Error bars represent mean \pm SD. P values were calculated using the Student's paired two-tailed t test. $*P < 0.05$.

lung fibroblasts were cultured on IPF-ECM, YAP nuclear localization was reduced (inactive YAP) (Figure 3A), along with reduced expression of YAP transcriptional targets (Figure 3B). Although YAP mRNA abundance is not influenced by ECM type (3), IPF-ECM significantly decreased YAP protein levels (Figure 3C). YAP downregulation by IPF-ECM is in accord with a possible mechanistic relationship between YAP and one of its transcriptional targets, the gene encoding miR-29b-1/a (13). To examine this possibility, we introduced an miR-29b-1/a luciferase reporter (18) into lung fibroblasts and found that IPF-ECM caused a modest but significant suppression of miR-29b-1/a transcriptional activity (Figure 3D). This raised the possibility that fibroblast YAP deficiency on IPF-ECM might lead to decreased transcription of *miR-29b-1/a*.

Enforced YAP Expression in Fibroblasts Does Not Restore Mature miR-29 Expression on IPF-ECM

To determine whether restoring YAP would rescue miR-29 expression on IPF-ECM, we

transduced lung fibroblasts with one of two active YAP expression constructs. The first encoded a stably active YAP mutant—resistant to proteosomal degradation (YAP S127/381A [FLAG tagged]); and the second encoded a constitutively active and stable YAP mutant (5SA-S61/109/127/164/381A [Myc tagged]) (19) (Figure 4A). As evidence that we achieved YAP gain of function in both cases, YAP transcriptional targets, including primary-precursor (Pri-Pre) miR-29a, were all upregulated on IPF-ECM (Figures 4B and 4C). As a control, we examined the impact of YAP gain of function on miR-29b-2/c, which does not contain a YAP-responsive regulatory element (18), and found its transcript abundance to be decreased—an effect that may represent an indirect effect of YAP gain of function. Despite increases in Pri-Pre miR-29a, mature miR-29 species remained unchanged after YAP gain of function (Figure 4D). YAP knockdown in lung fibroblasts on Ctrl-ECM had no effect (Figure E6). Thus, the inability of YAP gain of function to rescue mature miR-29 expression in

fibroblasts on IPF-ECM, despite increasing the levels of its primary/precursor forms, pointed downstream to deregulation of miR-29 processing as a candidate mechanism by which IPF-ECM suppresses miR-29.

IPF-ECM Suppresses the MicroRNA Processing Machinery

Processing of microRNA occurs cotranscriptionally, and processing of primary microRNA into precursor microRNA is a better predictor of mature microRNA abundance than transcriptional regulation alone (20). Prior work using mouse fibroblasts indicates that miR-29 expression depends on Drosha, Exportin-5, and Dicer1 (21), key components of the canonical microRNA processing machinery (Figure 5A). Of note, Ago2 (Argonaute-2), another component of the microRNA processing pathway, is reduced in IPF (22). To determine whether IPF-ECM altered microRNA processing, we measured Pri-Pre and mature miR-29a and -29c abundance (representing the two miR-29 genes) on ECM (Figure 5B). Pri-Pre miR-29 abundance increased on IPF-ECM, strongly implicating a downstream block in microRNA processing, particularly in view of the decreased transcription observed for *miR29b-1/a* on IPF-ECM. We therefore sought to determine whether IPF-ECM regulated Dicer1, Ago2, Drosha, or Exportin-5. IPF-ECM suppressed steady-state levels of Ago2, Drosha, and Dicer1, whereas Exportin-5 levels did not consistently change (Figure 5C, Figure E7). As a control, we examined the expression of three noncanonically processed microRNAs on IPF-ECM. Among the three (miR-320a, -451, and -484) (21), two of the three noncanonically processed microRNAs were unaltered by ECM type (Figure E8). As a control for internal consistency, we found that fibroblast expression of Dicer1 and other components of the microRNA processing machinery did not differ between soft and stiff polyacrylamide gels (Figure E9). Taken together, our experiments identified a microRNA processing defect as central to the suppression of fibroblast miR-29 expression by IPF-ECM.

Dicer1 Expression Is Reduced in Cells Comprising the Myofibroblast-Rich Core of the Fibroblastic Focus

Our experiments show that deregulation of lung fibroblast miR-29 expression

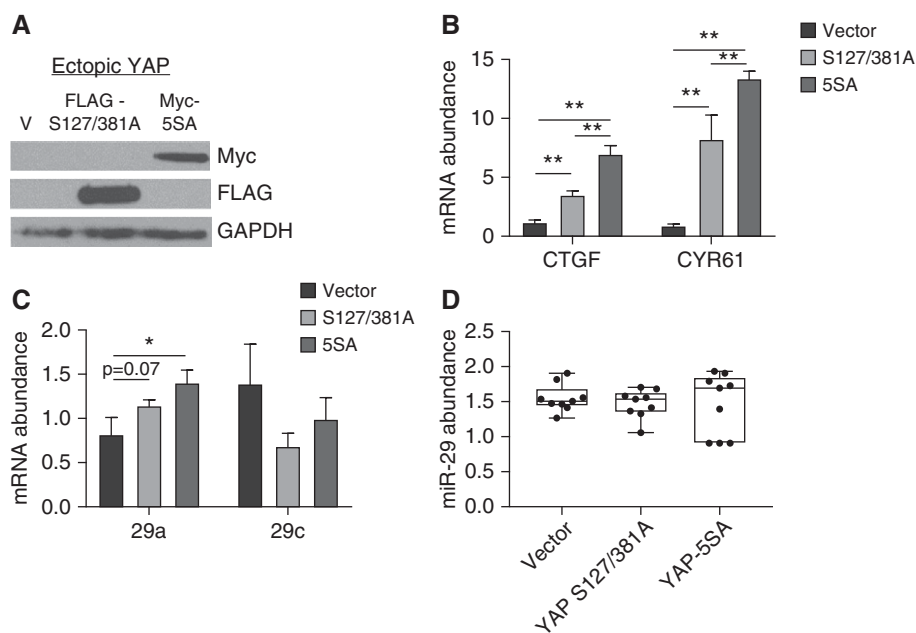


Figure 4. Enforced YAP (yes-associated protein) expression does not restore mature miR-29 (microRNA-29) expression on idiopathic pulmonary fibrosis (IPF)–extracellular matrix (ECM). (A–D) Fibroblasts were transduced with empty vector, YAP S127/381A–FLAG-tagged, or YAP 5SA–MYC-tagged and cultured on IPF-ECM for 18 hours. (A) Ectopic YAP expression was analyzed by immunoblot for anti-FLAG and anti-MYC. (B) YAP target genes CTGF and CYR61 were quantified by quantitative PCR (qPCR) normalized to GAPDH. (C) Primary-precursor miR-29a and -29c were quantified by qPCR normalized to GAPDH; (D) mature miR-29a, -29b, and -29c were quantified by qPCR normalized to RNU6 ($n = 2$, representative experiment shown). Error bars represent means \pm SD for B and C, and a box-and-whisker plot is shown for D. P value was calculated using a one-way ANOVA test followed by a Tukey test. $^*P < 0.001$, $^{**}P < 0.0001$.

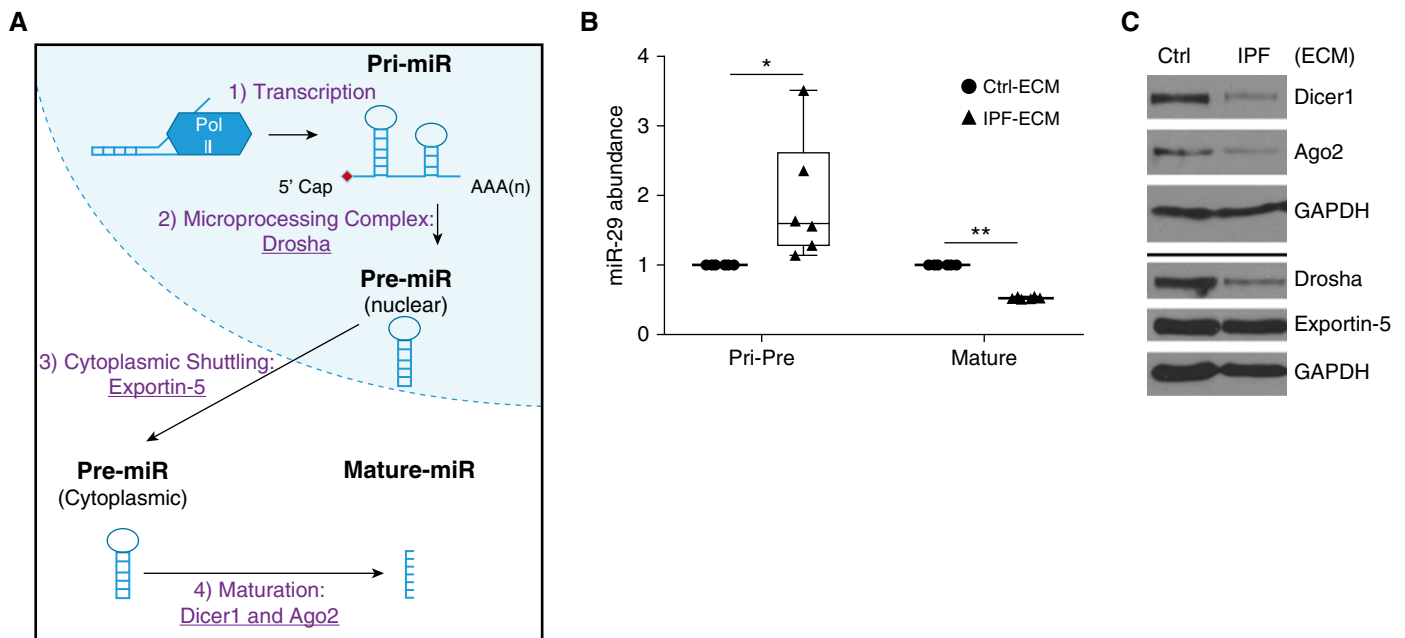


Figure 5. Idiopathic pulmonary fibrosis (IPF)–extracellular matrix (ECM) suppresses the microRNA processing machinery. (A) MicroRNA biogenesis schematic: 1) microRNAs are transcribed into primary microRNA (Pri-miR), 2) processed into precursor microRNA (Pre-miR) by the microprocessor complex (including Drosha), 3) actively shuttled from the nucleus to the cytoplasm by Exportin-5, and 4) processed into mature microRNAs by Ago2 and Dicer1. (B) Fibroblasts were cultured on ECM for 18 hours and quantitative PCR was used to analyze the grouped values of Pri-Pre and mature microRNA-29a (miR-29a) and miR-29c normalized to GAPDH or RNU6, respectively ($n = 3$ cell lines, mean value shown normalized to control [Ctrl]-ECM [set to 1]). Data are shown as a box-and-whisker plot, and P value was calculated using the Student's paired t test. * $P < 0.05$, ** $P < 0.0001$. (C) Fibroblasts were cultured on ECM for 24 hours. Shown are immunoblots for Dicer1, Ago2, Drosha, Exportin-5, and GAPDH ($n = 1$ cell line).

on IPF-ECM results from defects in microRNA processing. However, the microRNA processing machinery is a complex multicomponent apparatus, precluding efficient gain- and loss-of-function experiments involving each component singly or in combination. To direct our search for the microRNA processing step underlying the *in vivo* biology in IPF, we analyzed expression of microRNA processing components in the myofibroblast-rich core of the fibroblastic focus in IPF specimens (23). We analyzed serial sections for: histology (hematoxylin and eosin), procollagen I (a nascent form of collagen I and an miR-29 target), Ago2, Dicer1, Exportin-5, and Drosha. We consistently found that the myofibroblast-rich core of fibroblastic foci (defined by procollagen I reactivity) was deficient in Dicer1 compared with the focus perimeter and surrounding adjacent regions, whereas we found no consistent differences in Ago2, Exportin-5, or Drosha ($n = 7$ IPF specimens; Figure E10).

Guided by this initial analysis, we serially sectioned IPF specimens to further explore Dicer1 expression at both the

protein and RNA level. Serial sections (four tissue sections from one patient, 4 μ m each) were analyzed for morphology (Figure 6A), procollagen I (Figure 6B), Dicer1 protein (Figure 6C), and Dicer1 mRNA (*in situ* hybridization by RNAscope; Figure 6D). We examined a region of active collagen synthesis within the myofibroblast-rich focus core (dashed outlined box) and the focus perimeter (solid outlined box) with higher magnification (Figures 6B–6D, middle and right panels). The cells within the myofibroblast-rich core of the fibroblastic focus showed lower expression of both Dicer1 protein and mRNA (visualized as discrete brown dots) than cells at the focus perimeter. We quantified Dicer1 mRNA expression in six IPF lung specimens by enumerating the number of dots per cell within the myofibroblast-rich core compared with the focus perimeter (Figure 6E). Cells within the myofibroblast-rich core had significantly lower levels of Dicer1 mRNA expression than cells at the focus perimeter (Poisson regression, $P < 0.0001$). Taken together, our data implicate a deficiency of Dicer1 in the myofibroblast-rich core region of the fibroblastic focus

where active collagen synthesis is taking place (on the basis of procollagen I expression) in the *in vivo* mechanism of the IPF-ECM-mediated microRNA processing defect.

IPF-ECM Increases the Association of the Dicer1 Transcript with the RNA-Binding Protein AUF1

Available published literature points to control of Dicer1 mRNA levels by the RNA-binding protein AUF1 (AU-binding factor 1) (24). AUF1 binds to AU-rich elements in the Dicer1 transcript and recruits the mRNA degradation machinery, leading to decreased steady-state levels of the transcript. If this mechanism is operating in IPF, then the association of AUF1 with the Dicer1 transcript should increase on IPF-ECM. To test this possibility, we cultured primary human lung fibroblasts on IPF- and control-ECM and quantified AUF1 binding to Dicer1 mRNA through RNA immunoprecipitation (Figure 7). Consistent with this hypothesis, IPF-ECM increased the association of AUF1 with Dicer1 mRNA more than fivefold compared with control-ECM ($P < 0.05$ one-sided Mann-Whitney U test).

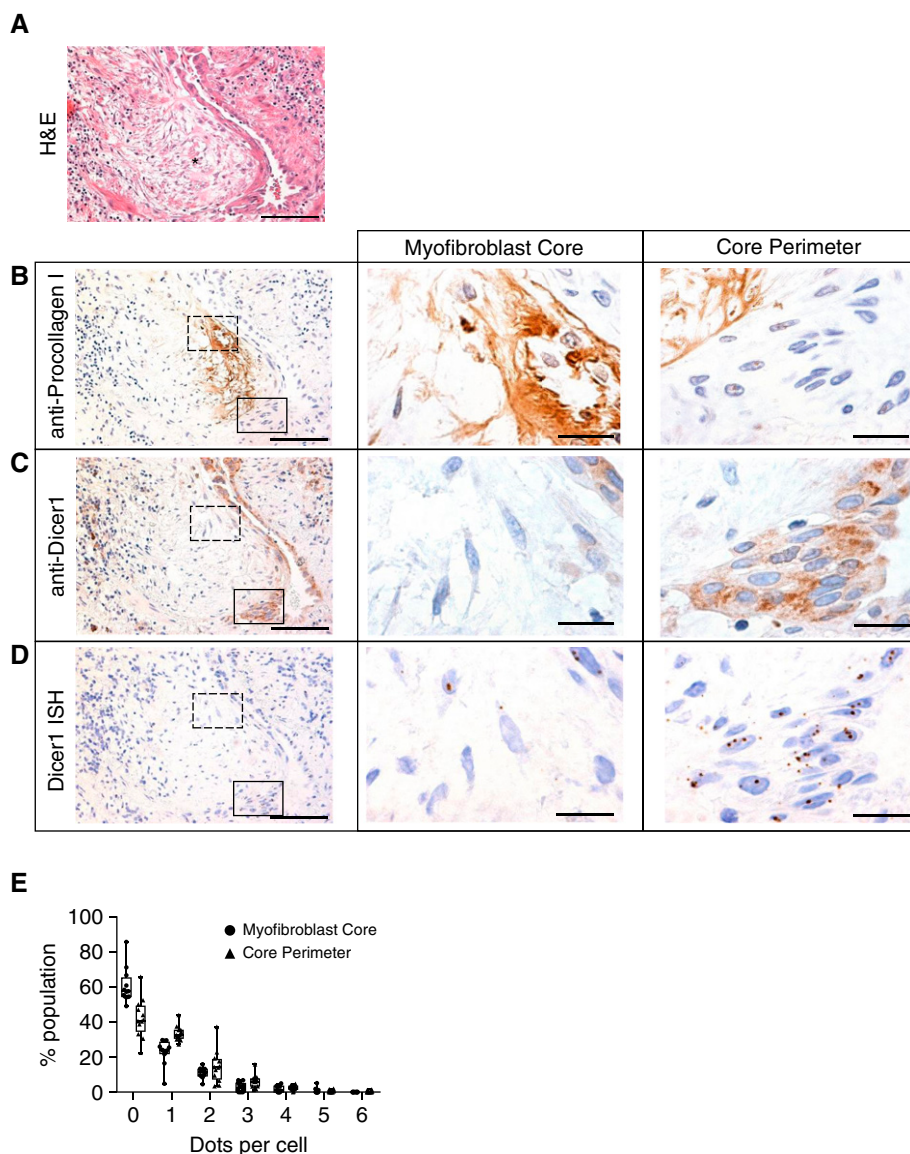


Figure 6. Regions of the lung actively synthesizing collagen are deficient in Dicer1. An idiopathic pulmonary fibrosis (IPF) specimen was serially sectioned at 4 μm and processed for histology and immunohistochemistry. (A) Hematoxylin and eosin (H&E) image with an asterisk labeling a fibroblastic focus. (B–D, left panels) Immunostain for anti-procollagen I (B), anti-Dicer1 (C), and *in situ* hybridization by RNAscope for Dicer1 mRNA (D). (B–D, middle and right panels) The myofibroblast core (dashed outlined box in left panels) and focus perimeter (solid outlined box in left panels) were reimaged at higher-power magnification. Scale bars represent 100 μm (left panels) or 20 μm (middle and right panels). (E) Quantification of RNAscope data. We enumerated dots within cells in the myofibroblast core or core perimeter shown as a frequency distribution (percentage population). Poisson regression, $P < 0.0001$ ($n = 6$ patients with IPF [12 fibroblastic foci total, 1–3 fibroblastic foci analyzed per patient]).

Dicer1 Knockdown Decreases Mature miR-29 Abundance and Increases Expression of miR-29 Target Genes on Ctrl-ECM

If Dicer1 deficiency is central to the mechanism leading to reduced miR-29 levels in IPF, then decreasing Dicer1 levels in lung fibroblasts on Ctrl-ECM should

replicate the biology observed on IPF-ECM. Stable Dicer1 knockdown in lung fibroblasts was achieved by transducing cells with a lentiviral-based shRNA (Figure 8A). In accord with a causal role, Dicer1 suppression decreased miR-29 abundance in lung fibroblasts on Ctrl-ECM (normalized to miR-451, which is processed

independently of Dicer1) (21) (Figure 8B), leading to increased secretion of miR-29 target genes (Figure 8C). We independently replicated this result in a second lung fibroblast line (Figure E11). To test whether restoring Dicer1 would rescue fibroblast miR-29 expression on IPF-ECM, we attempted to overexpress Dicer1 in two primary fibroblast lines (and in a lung cancer line A549 as a nonfibroblast control); however, in each case, all cells detached from the substratum and showed morphological evidence of toxicity within 48 hours after gene delivery. This precluded analysis of fibroblast Dicer1 gain of function on IPF-ECM. These data identify decreased Dicer1 processing of precursor forms of miR-29 in the mechanism by which IPF-ECM decreases fibroblast miR-29 expression.

Dicer1 Knockdown Imparts Fibroblasts with Fibrogenicity *In Vivo*

Having shown that Dicer1 deficiency in primary human lung fibroblasts is sufficient to decrease all three species of miR-29 and increase ECM synthesis *in vitro*, we next sought to determine whether these same Dicer1-deficient fibroblasts would display increased ECM production *in vivo* in the absence of any other cues. We considered using a lung fibroblast-specific conditional Dicer1 knockout (KO) mouse model for this purpose but chose not to use this model on the basis of two considerations. First, the effect of Dicer1 KO in mouse lung fibroblasts may not be comparable to Dicer1 deficiency in primary human lung fibroblasts, which could differ profoundly from those in mouse cells when modeling cell-autonomous functions (25). Second, studies in cancer using Dicer1 KO mice show that the Dicer1-null state inhibits tumor formation, a cell-autonomous function, whereas Dicer1 haploinsufficiency is permissive (26, 27). Therefore, we took a direct approach to test whether Dicer1-deficient primary human lung fibroblasts would display cell intrinsic/autonomous fibrogenicity using two *in vivo* xenograft model systems specifically designed for this purpose.

We previously described the use of zebrafish embryos as a simple and rapid *in vivo* xenograft system for assessing lung fibroblast fibrogenicity (28, 29). In control xenografts injected with fibroblasts transduced with nonsilencing scrambled shRNA, there were scattered procollagen

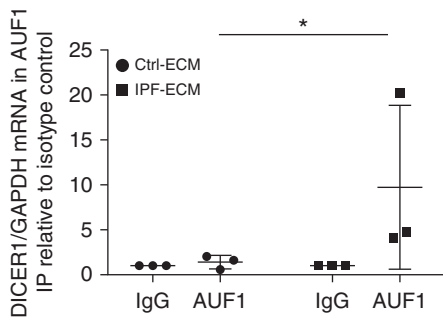


Figure 7. Idiopathic pulmonary fibrosis (IPF)–extracellular matrix (ECM) increases the association of RNA binding protein AUF1 with Dicer1 mRNA. RNA-immunoprecipitation (RNA-IP) was performed ($n = 3$ cell lines) against the RNA binding protein AUF1 (or isotype control, IgG) on lysates from cells cultured on control (Ctrl)- or IPF-ECM, and the amount of coprecipitated Dicer1 mRNA was quantified by quantitative PCR. Dicer1 mRNA was normalized to immunoprecipitated GAPDH mRNA levels (a highly abundant transcript to control for nonspecific associations). Dicer1/GAPDH expression levels are displayed relative to the isotype control (IgG) precipitation from the corresponding ECM type. Error bars represent SD, and P value was calculated using a one-sided Mann-Whitney U test. $*P = 0.05$.

I–expressing cells at the periphery of the graft, with only sparse procollagen I expression in the graft core (Figure 9A). In contrast, xenografts injected with

fibroblasts transduced with Dicer1 shRNA (Dicer1-KD) displayed prominent procollagen I expression throughout (Figure 9B). Quantification by image analysis indicated a significant increase in human procollagen I expression in xenografts containing Dicer1-KD fibroblasts compared with those with nonsilencing scrambled shRNA control (Figure 9C).

As an independent assessment of *in vivo* fibrogenicity, we tested Dicer1-KD fibroblasts in a mouse tail vein injection xenograft model. In this model, IPF lung fibroblasts produce prominent angiocentric fibrotic lesions, whereas control lung fibroblasts do not (28, 30). The lungs of mice receiving fibroblasts transduced with nonsilencing scrambled shRNA ($n = 8$) produced no morphological lesions (Figure 9D, left panels), a result consistent with our prior report using unaltered primary lung fibroblasts (28). In sharp contrast, the lungs from four out of eight mice injected with Dicer1-KD fibroblasts developed fibrotic lesions ($P < 0.04$), similar in morphology to those formed by IPF lung fibroblasts (28) (Figure 8D, middle and right panels). The largest of these fibrotic lesions spanned 300 μm at the 13-day time point (Figure E12). Thus, Dicer1 deficiency—even in the absence of cues

from a fibrotic ECM—is sufficient to confer human lung fibroblasts with cell-autonomous fibrogenicity in two *in vivo* xenograft models.

Discussion

Here we show that IPF-ECM inhibits lung fibroblast miR-29 expression upstream at the level of transcription and downstream at the processing step by suppressing Dicer1. Dicer1 deficiency suppresses lung fibroblast miR-29 expression on control ECM and confers lung fibroblasts with cell-autonomous fibrogenicity *in vivo*. We provide strong validation for our findings by showing that the cells in the myofibroblast-rich core of the IPF fibroblastic focus, where active collagen synthesis is taking place, display reduced levels of Dicer1 compared with cells comprising the focus perimeter. These data identify Dicer1 deficiency as a critical missing step in the mechanism of the IPF-ECM–driven profibrotic feedback loop, providing a new pathway to exploit for stopping fibrosis progression.

Several pathways can regulate miR-29 expression (7); however, we began our studies on the basis of the prevailing hypothesis in the field that ECM stiffness transduced through YAP could explain miR-29 deficiency in IPF. This concept derived from studies showing that stiffness drives lung fibroblast ECM production in a YAP-dependent manner on hydrogels (9), that stiff IPF-ECM drives fibroblast ECM production by deregulation of miR-29 (3), and that YAP regulates miR-29 expression (13) and microRNA processing (14), establishing a mechanistic link. When we compared fibroblast YAP and miR-29 expression on soft versus stiff hydrogels (a 2D system) to YAP and miR-29 expression on Ctrl-ECM versus IPF-ECM (a 3D system), stiff 2D hydrogels activated YAP and increased miR-29 levels, whereas IPF-ECM inactivated YAP and decreased miR-29 levels. This excluded stiffness as the primary property of IPF-ECM transduced by fibroblasts to deregulate YAP and miR-29.

Although these results were unexpected, they point to other ECM and cell surface properties that might play a role. These include dimensionality, viscoelasticity, cell–cell interactions, and

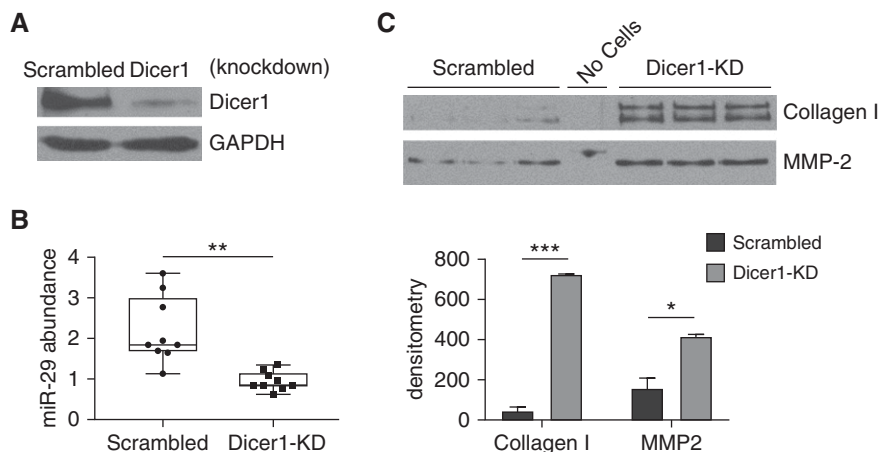


Figure 8. Dicer1 knockdown in fibroblasts decreases mature miR-29 (microRNA-29) abundance on control extracellular matrix. Fibroblasts were transduced with Dicer1 shRNA or scrambled control to establish stable expression. (A) Shown is an immunoblot for Dicer1. (B and C) Equal numbers of transduced cells were cultured on control extracellular matrix for 18 hours. Medium was removed and equal volume of serum-free medium was added to each reaction for 8 additional hours. (B) Quantitative PCR for mature miR-29a, -29b, and -29c normalized to miR-451. Data are shown as a box-and-whisker plot, and P value was calculated using the Student's two-tailed t test. (C) Equal volumes of conditioned medium were analyzed by immunoblot for collagen I and MMP-2 ($n = 2$, representative experiment shown in triplicate). Densitometry values are shown in the lower panel, with error bars representing the SD, and P value was calculated using the Student's two-tailed t test. $*P < 0.01$, $**P < 0.001$, $***P < 0.0001$. KD = knockdown.

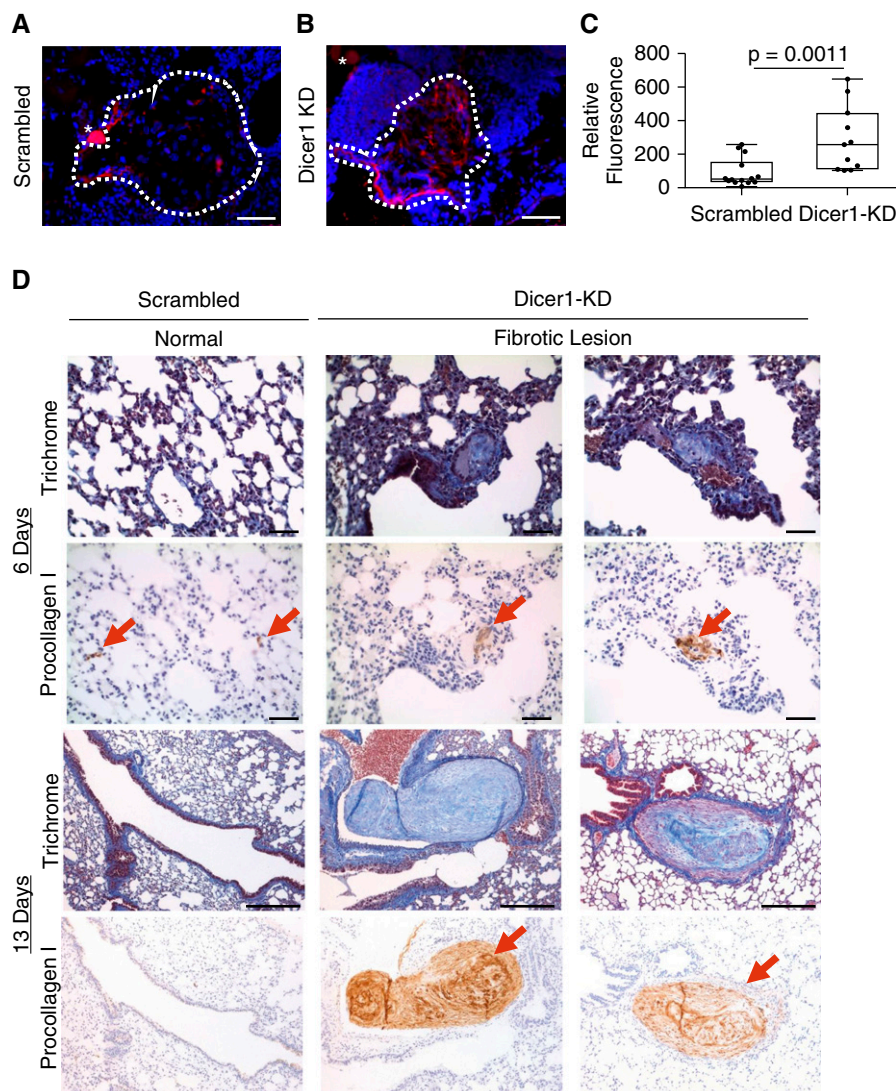


Figure 9. Dicer1 knockdown imparts fibroblasts with fibrogenicity *in vivo*. (A–C) Zebrafish xenograft assay: 10^2 scrambled control or Dicer1-knockdown (KD) fibroblasts (cells from the same population of lung fibroblasts used in Figure 8) were xenografted into each zebrafish embryo, which was incubated for 46 hours, anesthetized, and fixed before analysis. Representative xenograft images of (A) scrambled control or (B) Dicer1-KD fibroblasts immunostained for human procollagen I (red) counterstained with DAPI (graft DAPI-positive area outlined by dotted white line, scale bar represents $50\ \mu\text{m}$, asterisk indicates sectioning artifact: a yolk granule with autofluorescence). (C) A Fire LUT was applied using ImageJ to the unaltered images to quantify relative procollagen fluorescence, corrected to a background uninvolved area from the same image. Shown is a box-and-whisker plot of relative procollagen fluorescence with P values calculated using the Wilcoxon sum-rank test ($n = 13$ scrambled control and $n = 11$ Dicer1-KD zebrafish xenografts, $P = 0.0011$). (D) Mouse xenograft assay: 10^6 scrambled control or Dicer1-KD fibroblasts (cells from the same population of lung fibroblasts used in Figure 8) were injected by tail vein into mice and lungs were harvested after 6 and 13 days ($n = 4$ scrambled control and $n = 4$ Dicer1-KD per time point for a total of 16 mice). P value was calculated using Fisher exact test ($P = 0.04$). Trichrome and procollagen I immunostain (red arrows mark human fibroblasts) identify fibrotic lesions (scale bar represents $50\ \mu\text{m}$ for 6-day time point, or $200\ \mu\text{m}$ for 13-day time point).

cyclic stretch. In experiments examining mesenchymal stromal cell (MSC) YAP expression in response to substratum dimensionality (31), stiffness drove YAP

activation in a 2D system; whereas stiffness inactivated YAP in a 3D system. This result is in accord with our data, which showed fibroblast YAP activation on

stiff 2D gels but YAP inactivation on IPF-ECM. In addition, independent of substratum stiffness or dimensionality, MSC YAP activation is driven by increased viscoelasticity (32, 33), a parameter not yet assessed in the IPF lung. As an additional consideration, the YAP response to MSC mechanosensing of matrix stiffness is dampened by an order of magnitude when MSC N-cadherin (mimicking cell–cell interactions) is ligated (34). It is also worth noting that the constant strain and relaxation of the lungs during respiration represent a potentially important set of forces. Mammary epithelial cells activate YAP in response to cyclic stretch (35), and cyclic stretch and compression in periodontal ligament cells regulate miR-29 and downstream gene expression (36). Together, these studies illustrate the complexity of the mechanosensing–mechanotransduction axis, highlighting a critical gap in our understanding of fibrosis progression in IPF.

Dicer1 can act as both a tumor suppressor and oncogene (37). Global microRNA deregulation due to a microRNA processing defect is an established theme in cancer (38) and has been implicated in IPF (22, 39). In accord with Dicer1 haploinsufficiency supporting cell autonomy in cancer, we found that experimentally induced Dicer1 deficiency in human lung fibroblasts decreased miR-29 abundance, increased collagen production, and supported cell-autonomous fibrogenicity in zebrafish and mouse xenografts. Thus, both cancer and IPF exploit decreases but not ablation of the terminal steps in microRNA processing to stabilize cell-autonomous pathology. Another emerging function of Dicer1 is its role in DNA damage repair (26, 40), which we speculate might play a dual role in IPF progression. Recent data indicate that cellular senescence markers are expressed within the fibroblastic focus (41), and there is extensive crosstalk between DNA damage repair and cellular senescence (42). Thus, our study provides strong support for the concept that the IPF fibroblastic focus is highly polarized, with Dicer1 deficiency restricted to the myofibroblast-rich core of the fibroblastic focus functioning as a driver of fibrosis progression.

The mechanisms regulating Dicer1 expression remain incompletely defined. Our data support a role for the RNA binding protein AUF1, which associates with the

3' untranslated region of RNA to recruit the RNA degradation machinery (24). We found that IPF-ECM increases binding of AUF1 to the Dicer1 transcript more than fivefold, providing an explanation for some of the decrease in Dicer1 transcript we observed. Another possible mechanism is suggested by studies relating cell density to microRNA processing; nuclear YAP was necessary for processing precursor microRNAs into their mature forms (43). The microRNA Let-7, however, did not follow this trend. In the absence of nuclear YAP, Let-7 accumulates and targets Dicer1 mRNA (which contains Let-7 target sites), leading to a reduction in Dicer1 levels and defective microRNA processing. This is relevant because Let-7 levels are altered in IPF lung tissue (39). However, the focus of studies to date has

been whole lung tissue, and it remains to be determined whether Let-7 is increased within the procollagen I rich focus core where Dicer1 levels are low.

Although the underlying ECM properties that generate and maintain the polarity of the fibroblastic focus are not defined, one approach to elucidating this information would be to develop a comprehensive tissue atlas that combines mechanical measurements with cell identity and cell biology region by region. Although on average the IPF lung is stiffer than control, and there are some regional data available using atomic force microscopy, there are no data in IPF in which ECM mechanical properties (static and dynamic), topography, and chemistry have been coregistered to cell type and cell biology. Such data have proved highly informative in

cancer biology (44). Given the spatial heterogeneity of the fibrotic process in IPF, the importance of mechanotransduction in regulating cellular functions relevant to fibrosis, and the striking polarity of the fibroblastic focus, we conclude that studies connecting mechanics to cell biology region by region will be important to understand the molecular basis for fibrosis progression in IPF. ■

Author disclosures are available with the text of this article at www.atsjournals.org.

Acknowledgment: The authors thank Daniel J. Tschumperlin and Delphine Sicard for assistance in characterizing ECM mechanical properties and Vitaly Polunovsky for helpful suggestions and critical review of the manuscript. Any opinions, findings, and conclusions or recommendations expressed in this material are those of the authors.

References

- Booth AJ, Hadley R, Cornett AM, Dreffs AA, Matthes SA, Tsui JL, *et al.* Acellular normal and fibrotic human lung matrices as a culture system for in vitro investigation. *Am J Respir Crit Care Med* 2012;186:866–876.
- Herrera J, Henke CA, Bitterman PB. Extracellular matrix as a driver of progressive fibrosis. *J Clin Invest* 2018;128:45–53.
- Parker MW, Rossi D, Peterson M, Smith K, Sikström K, White ES, *et al.* Fibrotic extracellular matrix activates a profibrotic positive feedback loop. *J Clin Invest* 2014;124:1622–1635.
- Pandit KV, Corcoran D, Yousef H, Yarlagadda M, Tzouveleakis A, Gibson KF, *et al.* Inhibition and role of let-7d in idiopathic pulmonary fibrosis. *Am J Respir Crit Care Med* 2010;182:220–229.
- Roderburg C, Urban GW, Bettermann K, Vucur M, Zimmermann H, Schmidt S, *et al.* Micro-RNA profiling reveals a role for miR-29 in human and murine liver fibrosis. *Hepatology* 2011;53:209–218.
- Lv L-L, Cao YH, Ni HF, Xu M, Liu D, Liu H, *et al.* MicroRNA-29c in urinary exosome/microvesicle as a biomarker of renal fibrosis. *Am J Physiol Renal Physiol* 2013;305:F1220–F1227.
- He Y, Huang C, Lin X, Li J. MicroRNA-29 family, a crucial therapeutic target for fibrosis diseases. *Biochimie* 2013;95:1355–1359.
- van Rooij E, Sutherland LB, Thatcher JE, DiMaio JM, Naseem RH, Marshall WS, *et al.* Dysregulation of microRNAs after myocardial infarction reveals a role of miR-29 in cardiac fibrosis. *Proc Natl Acad Sci USA* 2008;105:13027–13032.
- Liu F, Lagares D, Choi KM, Stopfer L, Marinković A, Vrbanac V, *et al.* Mechanosignaling through YAP and TAZ drives fibroblast activation and fibrosis. *Am J Physiol Lung Cell Mol Physiol* 2015;308:L344–L357.
- Rahaman SO, Grove LM, Paruchuri S, Southern BD, Abraham S, Niese KA, *et al.* TRPV4 mediates myofibroblast differentiation and pulmonary fibrosis in mice. *J Clin Invest* 2014;124:5225–5238.
- Marinković A, Liu F, Tschumperlin DJ. Matrices of physiologic stiffness potently inactivate idiopathic pulmonary fibrosis fibroblasts. *Am J Respir Cell Mol Biol* 2013;48:422–430.
- DuFort CC, Paszek MJ, Weaver VM. Balancing forces: architectural control of mechanotransduction. *Nat Rev Mol Cell Biol* 2011;12:308–319.
- Tumaneng K, Schlegelmilch K, Russell RC, Yimlamai D, Basnet H, Mahadevan N, *et al.* YAP mediates crosstalk between the Hippo and PI(3)K–TOR pathways by suppressing PTEN via miR-29. *Nat Cell Biol* 2012;14:1322–1329.
- Mori M, Triboulet R, Mohseni M, Schlegelmilch K, Shrestha K, Camargo FD, *et al.* Hippo signaling regulates microprocessor and links cell-density-dependent miRNA biogenesis to cancer. *Cell* 2014;156:893–906.
- Herrera JA, Peterson MS, Parker MW, Smith K, Henke CA, Bitterman PB. Hippo signaling pathway deregulation in IPF controls microRNA-29 expression [abstract]. *Am J Respir Crit Care Med* 2015;191:A5337.
- Huang X, Yang N, Fiore VF, Barker TH, Sun Y, Morris SW, *et al.* Matrix stiffness-induced myofibroblast differentiation is mediated by intrinsic mechanotransduction. *Am J Respir Cell Mol Biol* 2012;47:340–348.
- Cretu A, Castagnino P, Assoian R. Studying the effects of matrix stiffness on cellular function using acrylamide-based hydrogels. *J Vis Exp* 2010;42:e2089.
- Mott JL, Kurita S, Cazanave SC, Bronk SF, Werneburg NW, Fernandez-Zapico ME. Transcriptional suppression of mir-29b-1/mir-29a promoter by c-Myc, hedgehog, and NF-kappaB. *J Cell Biochem* 2010;110:1155–1164.
- Zhao B, Li L, Tumaneng K, Wang CY, Guan KL. A coordinated phosphorylation by Lats and CK1 regulates YAP stability through SCF(beta-TRCP). *Genes Dev* 2010;24:72–85.
- Conrad T, Marsico A, Gehre M, Orom UA. Microprocessor activity controls differential miRNA biogenesis in vivo. *Cell Reports* 2014;9:542–554.
- Kim Y-K, Kim B, Kim VN. Re-evaluation of the roles of DROSHA, Export in 5, and DICER in microRNA biogenesis. *Proc Natl Acad Sci USA* 2016;113:E1881–E1889.
- Oak SR, Murray L, Herath A, Sleeman M, Anderson I, Joshi AD, *et al.* A micro RNA processing defect in rapidly progressing idiopathic pulmonary fibrosis. *PLoS One* 2011;6:e21253.
- Xia H, Gilbertsen A, Herrera J, Racila E, Smith K, Peterson M, *et al.* Calcium-binding protein S100A4 confers mesenchymal progenitor cell fibrogenicity in idiopathic pulmonary fibrosis. *J Clin Invest* 2017;127:2586–2597.
- Abdelmohsen K, Tominaga-Yamanaka K, Skirantan S, Yoon JH, Kang MJ, Gorospe M. RNA-binding protein AUF1 represses Dicer expression. *Nucleic Acids Res* 2012;40:11531–11544.
- Rangarajan A, Weinberg RA. Opinion: comparative biology of mouse versus human cells: modelling human cancer in mice. *Nat Rev Cancer* 2003;3:952–959.
- Swahari V, Nakamura A, Baran-Gale J, Garcia I, Crowther AJ, Sons R, *et al.* Essential function of Dicer in resolving DNA damage in the rapidly dividing cells of the developing and malignant cerebellum. *Cell Reports* 2016;14:216–224.
- Kumar MS, Pester RE, Chen CY, Lane K, Chin C, Lu J, *et al.* Dicer1 functions as a haploinsufficient tumor suppressor. *Genes Dev* 2009;23:2700–2704.

28. Xia H, Bodempudi V, Benyumov A, Hergert P, Tank D, Herrera J, *et al.* Identification of a cell-of-origin for fibroblasts comprising the fibrotic reticulum in idiopathic pulmonary fibrosis. *Am J Pathol* 2014;184:1369–1383.
29. Benyumov AO, Hergert P, Herrera J, Peterson M, Henke C, Bitterman PB. A novel zebrafish embryo xenotransplantation model to study primary human fibroblast motility in health and disease. *Zebrafish* 2012;9:38–43.
30. Pierce EM, Carpenter K, Jakubzick C, Kunkel SL, Flaherty KR, Martinez FJ, *et al.* Therapeutic targeting of CC ligand 21 or CC chemokine receptor 7 abrogates pulmonary fibrosis induced by the adoptive transfer of human pulmonary fibroblasts to immunodeficient mice. *Am J Pathol* 2007;170:1152–1164.
31. Caliarì SR, Vega SL, Kwon M, Soulas EM, Burdick JA. Dimensionality and spreading influence MSC YAP/TAZ signaling in hydrogel environments. *Biomaterials* 2016;103:314–323.
32. Chaudhuri O, Gu L, Klumpers D, Darnell M, Bencherif SA, Weaver JC, *et al.* Hydrogels with tunable stress relaxation regulate stem cell fate and activity. *Nat Mater* 2016;15:326–334.
33. Chaudhuri O, Gu L, Darnell M, Klumpers D, Bencherif SA, Weaver JC, *et al.* Substrate stress relaxation regulates cell spreading. *Nat Commun* 2015;6:6364.
34. Cosgrove BD, Mui KL, Driscoll TP, Caliarì SR, Mehta KD, Assoian RK, *et al.* N-cadherin adhesive interactions modulate matrix mechanosensing and fate commitment of mesenchymal stem cells. *Nat Mater* 2016;15:1297–1306.
35. Codellia VA, Sun G, Irvine KD. Regulation of YAP by mechanical strain through Jnk and Hippo signaling. *Curr Biol* 2014;24:2012–2017.
36. Chen Y, Mohammed A, Oubaidin M, Evans CA, Zhou X, Luan X, *et al.* Cyclic stretch and compression forces alter microRNA-29 expression of human periodontal ligament cells. *Gene* 2015;566:13–17.
37. Kurzynska-Kokorniak A, Koralewska N, Pokornowska M, Urbanowicz A, Tworak A, Mickiewicz A, *et al.* The many faces of Dicer: the complexity of the mechanisms regulating Dicer gene expression and enzyme activities. *Nucleic Acids Res* 2015;43:4365–4380.
38. Lin S, Gregory RI. MicroRNA biogenesis pathways in cancer. *Nat Rev Cancer* 2015;15:321–333.
39. Pandit KV, Milosevic J, Kaminski N. MicroRNAs in idiopathic pulmonary fibrosis. *Transl Res* 2011;157:191–199.
40. Francia S, Michelini F, Saxena A, Tang D, de Hoon M, Anelli V, *et al.* Site-specific DICER and DROSHA RNA products control the DNA-damage response. *Nature* 2012;488:231–235.
41. Schafer MJ, White TA, Iijima K, Haak AJ, Ligresti G, Atkinson EJ, *et al.* Cellular senescence mediates fibrotic pulmonary disease. *Nat Commun* 2017;8:14532.
42. Sulli G, Di Micco R, d'Adda di Fagagna F. Crosstalk between chromatin state and DNA damage response in cellular senescence and cancer. *Nat Rev Cancer* 2012;12:709–720.
43. Chaulk SG, Lattanzi VJ, Hiemer SE, Fahlman RP, Varelas X. The Hippo pathway effectors TAZ/YAP regulate dicer expression and microRNA biogenesis through Let-7. *J Biol Chem* 2014;289:1886–1891.
44. Weaver VM. Cell and tissue mechanics: the new cell biology frontier. *Mol Biol Cell* 2017;28:1815–1818.